

Magnetic-resonance measurements on the 5A_2 excited state of the neutral vacancy in diamond

J. A. van Wyk

Department of Physics, University of the Witwatersrand, Johannesburg, Wits 2050, South Africa

O. D. Tucker, M. E. Newton,* and J. M. Baker

Department of Physics, University of Oxford, Clarendon Laboratory, Parks Road, Oxford OX1 3PU, United Kingdom

G. S. Woods

Central Selling Organisation Valuations Ltd., 17 Charterhouse Street, London EC1N 6RA, United Kingdom

P. Spear

Diamond Trading Company Research Centre, Belmont Road, Maidenhead SL6 6JW, United Kingdom

(Received 19 June 1995)

The ground state of the neutral vacancy in diamond is diamagnetic and therefore has not been studied by electron paramagnetic resonance (EPR). We report the observation of EPR from the 5A_2 excited state of the neutral vacancy by EPR when illuminating an electron-irradiated natural IaB diamond with ultraviolet light. EPR and electron nuclear double-resonance (ENDOR) measurements show that the center has tetrahedral symmetry and the effective electron spin $S=2$. ${}^{13}\text{C}$ ENDOR measurements on the nearest- and next-nearest neighbor atoms have been interpreted by a simple molecular orbital calculation. The unpaired electron population is predominately localized in the carbon dangling orbitals. Our calculations suggest that the relaxation of the nearest-neighbor carbon atoms away from the vacancy is greater for the 5A_2 excited state of V^0 than the 4A_2 ground state of V^- . The EPR signal has an unusual line shape which arises from a combination of small shifts in the positions of transitions between different M_S states and the anisotropic population of the different states. The electronic g shift of 0.0010(1) can be accounted for by spin-orbit coupling mixing the 3T_2 and 5A_2 states, which are separated by approximately 1 eV. The effect of illumination with monochromatic photons on the EPR has been studied of both ground state V^- and excited state V^0 . We propose that the excited V^0 is created by ionization of V^- rather than internal excitation in V^0 . The lifetime of the 5A_2 excited state was measured at helium temperatures by monitoring the decay of the EPR signal when the ultraviolet light was removed. Above about 100 K the EPR linewidth varied in an exponential fashion with an activation energy of about 40 meV.

I. INTRODUCTION

A. Irradiation damage in diamond

The defects created by irradiating diamond with particles of sufficient energy to displace atoms from their normal lattice sites have been studied continuously over the last 35 to 40 years by optical and electron paramagnetic resonance (EPR) spectroscopies. The field has been recently reviewed.¹ Apart from the nitrogen vacancy center^{2,3} and the negatively charged vacancy⁴ (V^-) EPR and related techniques have been remarkably unsuccessful at establishing definitive models for defects created by radiation damage or those formed by subsequent annealing. The technological interest stimulated by recent advances in the chemical vapor deposition of diamond has refreshed the desire to improve our understanding of defects and impurities in diamond. This paper reports the discovery of a paramagnetic center in diamond, observed after electron irradiation while illuminating the sample with uv light. The results presented in this paper show that this center is a paramagnetic excited state of the neutral vacancy.

B. The neutral vacancy in diamond

The GR1 optical absorption/luminescence band in diamond has long been identified with the neutral vacancy

(V^0).⁵ It is characterized by a zero-phonon line at 1.673 eV which has been identified with a 1E to 1T_2 transition (1E is the ground state).^{6,7} A much weaker line at 1.665 eV corresponds to a transition from a 1A state to the same 1T_2 state mentioned above.⁸ The temperature dependence of the intensities of the 1.665 and 1.763 eV lines indicates that the 1A_1 state is 8 meV above the 1E state.⁸ Considerable attention has been paid to the interaction of the electrons and the vibrational modes of V^0 and the consequences of the dynamic Jahn-Teller distortion are well understood.⁹ A set of transitions between 2.88 and 3.01 eV labeled GR2-GR8 arise from the neutral vacancy, but many of their properties are not understood.^{9,10}

The vacancy may be modeled using the defect-molecule approach where it is assumed that the properties are determined by the electrons in the dangling orbitals on the neighbors of the vacancy. The T_d point group requires that these orbitals transform as a_1 and t_2 . In the neutral vacancy four electrons are accommodated in these orbitals. The configuration $a_1^2t_2^2$ (or t_2^4) gives rise to the states 1A_1 , 1E , 3T_1 , and 1T_2 , while the configuration $a_1^1t_2^3$ gives rise to the states 5A_2 , 3A_2 , 3E , 1E , 3T_1 , 1T_1 , 3T_2 , and 1T_2 . Determining the order of these energy levels is a taxing theoretical prob-

lem. The pioneering work of Coulson and Kearsley,¹¹ and subsequent theoretical calculations have shown that there are several possible ground states for the neutral vacancy in diamond, all with similar energies. As a consequence electron-electron correlation becomes important, not because it is exceptionally large but because there are several different states with similar energies.

Calculations on a perturbed vacancy identify the 3T_1 level of the unperturbed vacancy as being located up to 200 meV above the 1E ground state.¹² Combining the experimental and theoretical evidence we can order in increasing energy the 1E , 1A_1 , 3T_1 , and 1T_2 levels. Most theoretical calculations suggest that the 5A_2 state is one of the lowest in energy, but until now no measurements have been made on this state and its position has not been known.

Annealing experiments on diamond at temperatures between 600 and 750 °C have shown that neutral vacancies migrate with an activation energy of 2.3(3) eV.¹³

C. The negatively charged vacancy in diamond

In type Ia or Ib diamond irradiation with particles sufficiently energetic to create lattice vacancies produces a fraction of the vacancies in the negative charge state. The negatively charged vacancy is characterized by an optical absorption band called ND1 with a zero-phonon line at 3.149 eV which occurs between a 4A_2 ground state and a 4T_1 excited state at a tetrahedral center.^{14,8}

The $S=3/2$ spin state of the ground state has been confirmed by electron nuclear double resonance (ENDOR).⁴ The ${}^{13}\text{C}$ hyperfine coupling parameters show that the sum of the unpaired spin densities on the four nearest neighbors is approximately one, indicating that the electron delocalization away from the negatively charged vacancy is very small.

The relative intensities of the ND1 and GR1 bands can be sensitive to the illumination and annealing of the diamond,^{15,8} the effects depending on whether V^0 captures an electron, or V^- loses an electron (or captures a hole). No luminescence band has been observed from the 3.149 eV center, which has led to the conclusion that the excited state is unstable with respect to charge emission. The negatively charged vacancies undergo a reversible charge transfer process to the neutral state before they migrate.¹³ No experimental observations of the positively charged vacancy in diamond have been reported.

D. Vacancy centers in silicon

It is worthwhile when considering vacancies in diamond to pay attention to the studies of vacancies in silicon, even though vacancies in diamond and silicon show distinctly different properties. Our understanding of vacancies in silicon is primarily based on the paramagnetic resonance work of Watkins.¹⁶⁻¹⁸ Watkins analyzed the vacancy centers in silicon using a one electron defect molecule (concentrating on the dangling bonds) assuming that the electrons pair off whenever possible and that the Jahn-Teller effect is stronger than any corrections to the one electron model. Theory and experiment are in accord, the paramagnetic positively charged vacancy ($a_1^2t_2$) distorts to D_{2d} symmetry, as does the diamagnetic neutral vacancy ($a_1^2t_2$). The negatively

charged vacancy ($a_1^2t_2$) also observed by EPR distorts to C_{2v} symmetry (a mixed tetragonal and trigonal distortion). The ENDOR results of Sprenger *et al.*¹⁹ confirm the picture of the negatively charged vacancy determined by Watkins.

The static Jahn-Teller distorted V^0 and V^- centers in silicon are markedly different from the same centers in diamond which maintain their tetrahedral symmetry. As explained by Davies²⁰ one major difference between diamond and silicon is that the acoustic modes in diamond have abnormally high energies at the zone boundaries, consequently stabilizing the vacancies against a tetragonal distortion. In silicon the Jahn-Teller interaction is sufficiently large for a static distortion to occur whereas in diamond even though the Jahn-Teller energies are large only dynamic distortions result.

The vacancy in silicon is mobile well below room temperature, V^0 anneals out between 150 and 180 K and V^- anneals at approximately 75 K.²¹ It is well known that the vacancy production rate in *p*-type silicon is about an order of magnitude higher than in *n*-type material. The high mobility of self-interstitials in silicon means that recombination of vacancies and interstitials readily occurs unless the latter are trapped. The substitutional acceptor elements act as competitive traps for silicon interstitials, and become interstitial themselves.^{22,23} Little is known about self-interstitials in diamond, although they are generally presumed mobile well below room temperature. Davies *et al.*¹³ show that in type IaA diamond about 40% of the vacancies are created within a few atomic sites of the di-nitrogen *A* centers, and that in these diamonds vacancy production is enhanced.

The charge states V^{2+} , V^+ , and V^0 in silicon have been shown to form an example of a negative-*U* system.²⁴⁻²⁶ The addition of an extra electron lowers the total energy rather than raising it. This effect arises because the energy gain of Jahn-Teller distortion is larger than the repulsive energy of the electrons.

II. EXPERIMENT

A. The sample

The sample used in this study was a natural IaB diamond which had been cut and polished with two parallel {110} faces. It was originally irradiated with 2 MeV electrons to a dose of $9 \times 10^{17} \text{ cm}^{-2}$. A new center was present on illumination with uv light immediately after irradiation but grew stronger after moderate annealing. The sample was annealed at various temperatures, with a final anneal at 1500 °C for 1 hour. The new center annealed out at the same temperature as V^- . The diamond was then irradiated with the same electron dose as before and annealed at 600 °C for 10 minutes.

B. EPR/ENDOR spectrometer

EPR measurements were made at temperatures between 100 and 300 K using a Varian E-line X-band spectrometer in a standard configuration. Further EPR measurements were made at temperatures between 3.7 and 300 K using a Bruker TE₁₀₄ resonant cavity operating at about 9.65 GHz in conjunction with an Oxford Instruments ESR900 continuous flow cryostat. The EPR/ENDOR spectrometer used for the later measurements incorporated a standard reference arm microwave bridge and was built in the Clarendon Laboratory.

ENDOR measurements were made using a micro-ENDOR coil which was an integral part of the sample holder and could be inserted into the cold finger of the ESR900 cryostat. For the TE_{102} or TE_{104} rectangular modes the long leads of ENDOR coil (copper wire OD 0.25 mm) are perpendicular to the microwave E-field and positioned in or close to the nodal plane. By making the loop longer than the cavity its bottom can be positioned outside the cavity, but it was found that it was possible to have the coil carefully wound directly around the sample without degradation of the cavity quality factor. The rf coil should be positioned such that the rf field is perpendicular to the static Zeeman field. A simple housing was constructed which fitted onto the goniometer mounted on the cryostat, the rf input and output connections were made through vacuum tight SMA connectors, and the sample rod inserted through an O-ring seal at the top. The cavity and cryostat could be used without modification. For ENDOR and EPR measurements on optically excited centers a circular quartz rod with the sample glued to the end served the dual purposes of light guide and sample rod.

The study of transient signals is restricted by the time resolution of our continuous wave EPR/ENDOR spectrometer. The technique of field modulation (115 kHz) and lock in detection places a lower limit on the time resolution of about 200 μ s. The electronic shutter used to switch on or off the light has a response time of about 0.5 ms. Worthwhile measurements can be made only for transients with a characteristic lifetime of a few ms or longer.

C. Optical absorption measurements

Optical absorption measurements in the visible/uv were made with a Lambda 19 spectrophotometer. The sample was mounted in an Oxford Instruments liquid nitrogen cryostat (DN1704) and held at 77 K. The infrared absorption measurements were made at room temperature using a Perkin-Elmer 1710 infrared Fourier-Transform spectrometer.

III. RESULTS

A. Infrared and uv/visible optical-absorption measurements

It is apparent when observing the sample under an optical microscope that it is inhomogeneous. One region is much darker with a light green color and the other is clearer with a light blue tinge. The infrared absorption spectra in the one phonon region are shown in Fig. 1. The spectra were taken by masking off one of the different sectors of the diamond. Spectrum (a) from the dark region shows very strong absorption from B centers; this sector can be categorized as IaB. The current consensus is that the B center consists of four nitrogens around a vacancy.²⁷ Using the parameter determined by Woods and co-workers,²⁸ the concentration of nitrogen in the form of B centers is estimated to be 800 ppm. The peak at 1405 cm^{-1} originates from a C-H bend and is accompanied by a stronger line at the C-H stretch frequency (3107 cm^{-1}).²⁹ Spectrum (b) from the lighter region shows a much lower total absorption which is predominately from B centers with a small contribution from A centers. The A center consists of a pair of adjacent substitutional nitrogen atoms.³⁰ No platelet peak is observable in either region (a) or

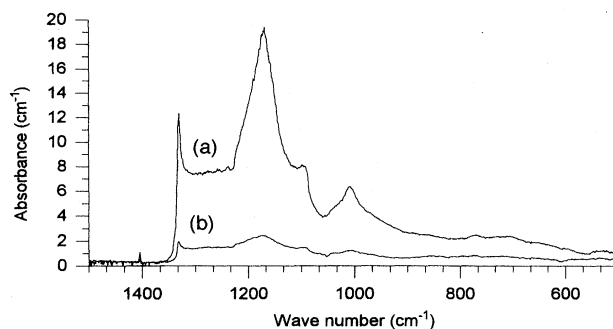


FIG. 1. Infrared absorption spectra taken at room temperature. Different regions of the sample are labeled (a) and (b). See the text for further details.

(b). Following the notation usually adopted for infrared characterization of diamond the specimen here can be characterized as *irregular*.

The uv/visible absorption spectra measured in regions (a) and (b) are shown in Fig. 2. The 1.673 eV and 3.149 eV zero-phonon lines of V^0 and V^- , respectively, are seen in both regions. The 2.463 eV zero-phonon line of the H3 center is seen in both regions but stronger in (b). The 2.498 eV zero-phonon line of the H4 center is clearly seen in region (a), but in region (b) it is much weaker and obscured by the phonon assisted structure on the H3 center. All the phonon lines in region (a) are broader than those in region (b). The widths of zero-phonon lines are predominately caused by random strain in the local environment of the defect. The wider zero-phonon lines in region (a) are probably caused by the very high concentration of B centers which is likely to be a major source of strain. The concentration of V^- ($[V^-]$) and the ratio $[V^-]/[V^0]$ is higher in region (a) than in region (b), indicating that there are more electron donors in region (a). During annealing some vacancies were captured by B centers producing H4 centers, and others captured by A centers producing H3 centers. The higher concentration of H4 in region (a) is consistent with the higher B center concentration measured by infrared absorption.

B. EPR spectra and angular variation

Figure 3(a) shows the EPR spectrum obtained without any illumination with the Zeeman field aligned parallel to a $[001]$

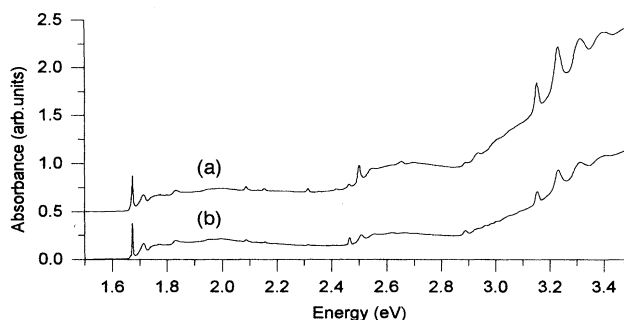


FIG. 2. Visible/uv absorption spectra taken at 77 K. Different regions of the sample are labeled (a) and (b). Spectrum (a) offset for clarity. See the text for further details.

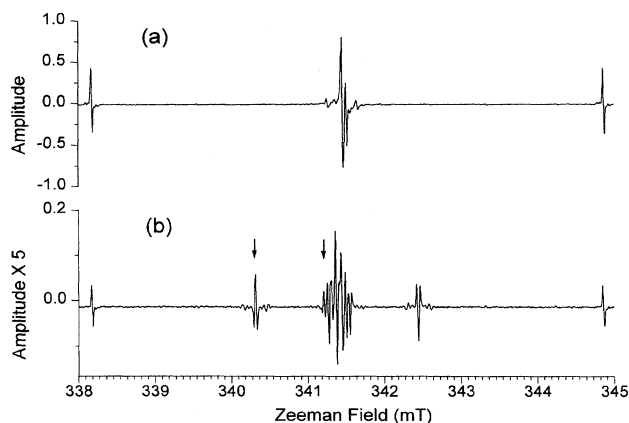


FIG. 3. EPR spectra taken at 5 K with Zeeman field oriented along a [001] crystallographic axis. The microwave frequency was approximately 9.6 GHz and 30 nW of microwave power incident on the TE₁₀₄ cavity. Spectra were taken (a) without illumination and (b) with the sample illuminated by the full spectrum from Hg lamp.

crystallographic axis. The characteristic spectrum from the neutral single substitutional nitrogen ([N-C]⁰) center is visible. A strong central line at $g=2.0027(1)$ from V^- centers is visible along with the associated hyperfine satellites from nearest-neighbor, next-nearest-neighbor, and possibly next-next-nearest-neighbor ¹³C atoms (natural abundance 1.1%). Comparison with a calibrated reference sample indicated that the concentrations of [N-C]⁰ and V^- are 0.40(8) ppm and 0.14(8) ppm, respectively.

When the sample is illuminated with the full light of a Hg arc lamp the EPR spectrum changes to that shown in Fig. 3(b). The V^- and [N-C]⁰ EPR signals are reduced in intensity and a new system is observed with what at first appears to be a strange line shape [Fig. 3(b)]. The line shape originates from the addition of components in absorption and

emission at slightly different resonant fields and is explained in Sec. IV B. The effect of light of different wavelengths is reported in Sec. III C. The angular variation of the position and intensity of the outer lines in a {110} plane is shown in Fig. 4; the variation in intensity with orientation is pronounced. The angular variation indicates a [111] axially symmetric hyperfine interaction, and ENDOR measurements (Sec. III E) identify ¹³C as the nucleus involved. There are four equivalent symmetry related sites. The solid curve in Fig. 4 was determined by least squares fitting the EPR and ¹³C ENDOR data to the spin Hamiltonian given in Eq. (1), all terms having their usual meaning:

$$\mathcal{H} = g\mu_B \mathbf{S} \cdot \mathbf{B} + \mathbf{S} \cdot \mathbf{A} \cdot \mathbf{I} - g_N \mu_N \mathbf{I} \cdot \mathbf{B}, \quad (1)$$

with $S=2$, $I=1/2$, $g=2.0033(1)$, and the parameters shown in Table I. The g value was determined by comparison to the [N-C]⁰ [2.0024(1)] (Ref. 31) and V^- [2.0027(1)] (Ref. 4) centers. The fitting was performed using EPR.FOR.³² It is not possible to determine the effective electron spin from the EPR spectra alone; analysis of the ENDOR data confirms that $S=2$ (Sec. III E). For a center with T_d symmetry no term $\mathbf{S} \cdot \mathbf{D} \cdot \mathbf{S}$ is required in Eq. (1). The absence of fine structure splitting arising from such a term is clear evidence for the T_d symmetry of the defect. However, with $S=2$ we should expect an additional term

$$\frac{a}{6} \left\{ S_x^4 + S_y^4 + S_z^4 - \frac{1}{5} S(S+1)(3S^2 + 3S - 1) \right\} \quad (2)$$

in Eq. (1). This term does not vanish in T_d symmetry and would produce a fine structure splitting; however, a is usually very small. Including this term in Eq. (1) does not improve the fit to the EPR transitions shown in Fig. 4. We estimate that $a < 1$ MHz which is too small to have an effect on the position of the EPR transitions.

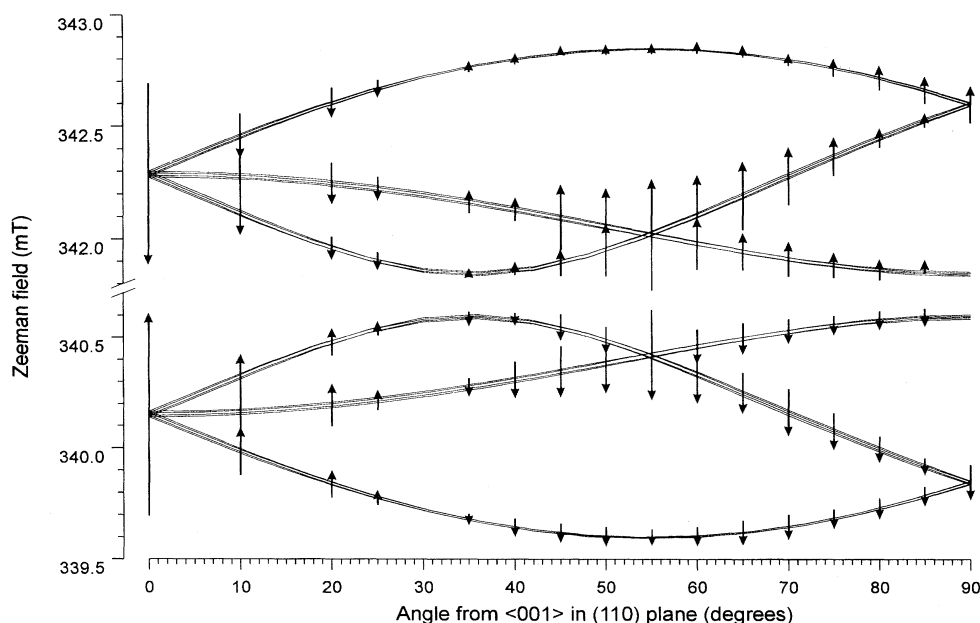


FIG. 4. Roadmap showing the positions of the nearest-neighbor ¹³C hyperfine lines from the ⁵A₂ state of V^0 when the magnetic field is rotated in a (110) plane away from [001]. The arrows show the intensity and phase of the EPR transitions and the solid curve shows the theoretical positions determined by fitting the EPR and ENDOR data.

TABLE I. Nearest (NN) and next-nearest (NNN) neighbor ${}^{13}\text{C}$ hyperfine constants, and the wave function parameters calculated from them, for the 4A_2 ground state of V^- and the 5A_2 excited state of V^0 . See text for further details. Hyperfine parameters for 4A_2 state of V^- taken from Isoya *et al.* [Phys. Rev. B **42**, 1436 (1992)].

| | A_{\parallel} (MHz) | A_{\perp} (MHz) | A_S (MHz) | A_p (MHz) | η^2 | λ^2 |
|---------------------|-----------------------|-------------------|-------------|---------------|----------|-------------|
| ${}^4A_2:V^-$ (NN) | 121.6 | 61.9 | 81.8 | 19.9 | 0.827 | 6.9 |
| ${}^4A_2:V^-$ (NNN) | 13.42 | 9.40,9.23 | 10.68 | ≈ 1.4 | 0.016 | 4.5 |
| ${}^5A_2:V^0$ (NN) | 91.13(9) | 35.03(5) | 53.73(5) | 18.70(3) | 0.753 | 12.2 |
| ${}^5A_2:V^0$ (NNN) | 12.0(1) | 8.36(6) | 9.6(1) | 1.2(1) | 0.014 | 4.4 |

EPR spectra around $g = 2.0033$ recorded with the Zeeman field parallel to [001], [111], and [110] crystallographic directions are shown in Fig. 5. The central transitions of the $[\text{N-C}]^0$ and V^- centers are indicated. The large line at $g = 2.0033(1)$ is only observed on illumination and is at the mean field of the outer ${}^{13}\text{C}$ satellites discussed above. It is therefore identified as belonging to the same defect, but one where all of the near-neighbor carbon atoms are ${}^{12}\text{C}$ so no hyperfine splitting is resolved. Assignment of the EPR spectra arising from the same defect with a single ${}^{13}\text{C}$ in a next-nearest-neighbor position (all other near neighbors are ${}^{12}\text{C}$) is difficult because the lines are weak, the line shape unusual, and many overlapping resonances are present. Simulations of the EPR spectra expected for centers with this single ${}^{13}\text{C}$ neighbor, using the hyperfine parameters determined by ENDOR (Table I), are shown in Fig. 5.

Further support for this assignment of transitions to next-nearest-neighbor ${}^{13}\text{C}$ atoms comes from the observation of weak satellites on either side of the main nearest-neighbor ${}^{13}\text{C}$ satellites [Fig. 6(a)]. These originate from defects with a single ${}^{13}\text{C}$ nearest neighbor and a single ${}^{13}\text{C}$ next nearest neighbor. An experimental spectrum with the applied Zeeman field parallel to [001] is shown in Fig. 6(a) together with simulations with [Fig. 6(d)] and without [Fig. 6(c)] a next-nearest-neighbor ${}^{13}\text{C}$ atom. Figure 6(b) is a sum of Figs. 6(d)

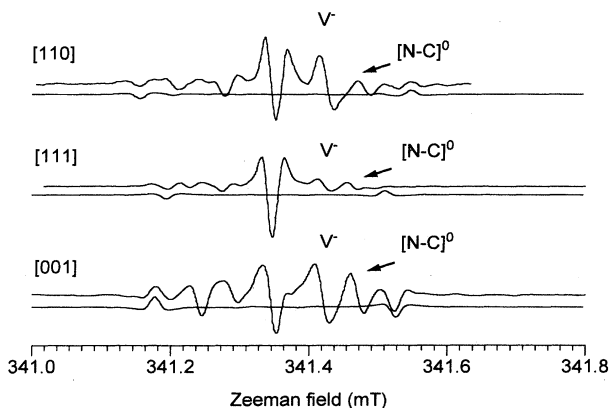


FIG. 5. The central regions of the EPR spectra of $[\text{N-C}]^0$, 4A_2 (V^-), and 5A_2 with the Zeeman field aligned along [001], [111], and [110] directions. The microwave frequency was approximately 9.6 GHz, the incident microwave power 30 nW, temperature 5 K, and the sample illuminated with the full spectrum of a Hg lamp. The traces beneath the experimental data show the simulated spectra resulting from hyperfine interaction with next-nearest-neighbor ${}^{13}\text{C}$ atoms.

and 6(c). Even without a ${}^{13}\text{C}$ next nearest neighbor weak satellites arise from forbidden transitions [Fig. 6(c)], but these are too weak to be useful in determining the effective electronic spin from the EPR spectra. It is also clear that weak transitions close to the main lines, probably from more distant ${}^{13}\text{C}$ neighbors, have yet to be accounted for.

The temperature dependence of the intensity of the EPR signal from the new center is unusual. Figure 7(a) shows the temperature dependence of the peak-to-peak line height of the lowest field transition labeled with an arrow in Fig. 3. The intensity increases rapidly as the temperature is reduced to about 100 K, but then remains constant down to 4 K. The behavior clearly does not follow the Curie-Weiss law.

C. Excitation energy dependence of EPR from the V^- ground state and the new EPR center

The data reported in Sec. III B were recorded with the full illumination of the Hg lamp. The effect of monochromatic light of energy 2.85(7) eV (436 nm), 3.1(1) eV (404 nm), and 3.4(1) eV (364 nm) on the intensity of the EPR signal of the V^- ground state and the new excited state center was mea-

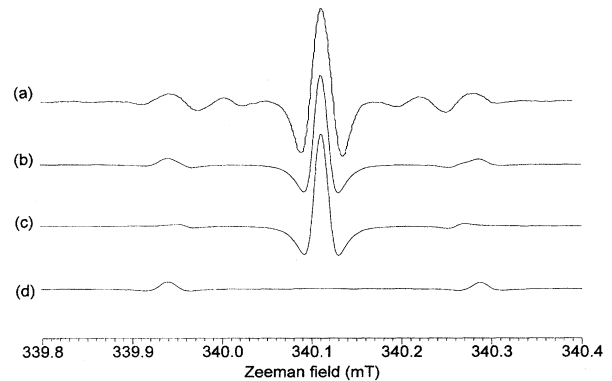


FIG. 6. (a) Expanded EPR spectrum showing the lowest field transition in Fig. 4 marked with an arrow. Microwave frequency was 9.6 GHz, incident microwave power 30 nW, temperature 5 K, and the sample illuminated with the full spectrum of the Hg lamp. (b) Simulation summing the spectra from a defect with a single nearest-neighbor ${}^{13}\text{C}$ atom and a defect with a nearest-neighbor and a next-nearest-neighbor ${}^{13}\text{C}$ atom [i.e., sum of spectra in (c) and (d)]. (c) Simulation of part of the EPR spectrum for defect with a nearest-neighbor ${}^{13}\text{C}$ atom and no next-nearest-neighbor ${}^{13}\text{C}$ atoms. (d) Simulation of part of the EPR spectrum for a defect with a nearest-neighbor and a next-nearest-neighbor ${}^{13}\text{C}$ atom.

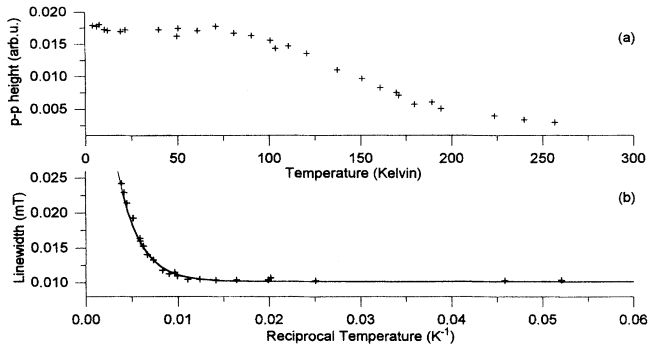


FIG. 7. (a) Temperature dependence of the peak line height for the lowest field nearest-neighbor ^{13}C hyperfine transition (Zeeman field along [001], microwave frequency 9.6 GHz, incident microwave power is 30 nW, and illumination with full spectrum of Hg lamp). (b) Variation of component linewidth with reciprocal temperature. The solid curve shows the fit to single exponential decay. See the text for further details.

sured at 298 and 5 K. For the measurements on V^- the sample was left in the dark at room temperature for several hours, and then illuminated in the sequence shown in Table II. When the light was applied or removed the signal changed relatively slowly (Sec. III D) but came to equilibrium within 5 minutes and no further changes were observed. If the sample had not been exposed to 2.85(7) eV light before illumination with 3.1(1) eV light then the V^- EPR was quenched irrespective of temperature. No EPR signal was observed from the new center with 2.85(7) eV light, but it was created with both 3.1(1) and 3.4(1) eV light, the signal strength being approximately identical with the two wavelengths.

D. Lifetime of the new excited state EPR center, quenching and recovery of the EPR from the V^- ground state, and the single substitutional nitrogen center

The following measurements were made with the full illumination of the Hg lamp. Figure 8 shows that the ampli-

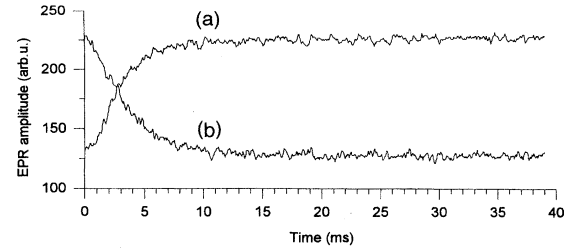


FIG. 8. Temporal dependence of EPR signal from $^5A_2 V^0$ on (a) illumination with full spectra of Hg lamp, or (b) subsequent removal of illumination. The Zeeman field is along [001] (set on lowest field nearest-neighbor ^{13}C hyperfine line), the microwave frequency is approximately 9.6 GHz, incident microwave power 0.3 mW, and the temperature is 5 K.

tude of the EPR signal from the new center decays rapidly when the excitation is removed and the intensity of the EPR signal saturates rapidly upon illumination. We define τ_d as the time constant for the decay of the EPR signal from the new center when the excitation is switched off, and τ_g as the time constant for the growth of the EPR signal from the new center when the excitation is switched on. The measured decay and growth times depend on the incident microwave power, at high microwave powers when the EPR signal is saturated the decay and recovery times are reduced. All times given in the text are determined by extrapolating to zero microwave power. Fitting the decay to a single exponential function ($\exp[-t/\tau_d]$) indicates that $\tau_d = 9.0(8)$ ms at 5.0 K. Fitting the growth on illumination to an increasing exponential function ($1 - \exp[-t/\tau_g]$) indicates that $\tau_g = 9.0(8)$ ms at 5.0 K. Measurements at temperatures up to 74 K show that τ_d remains approximately constant over this range.

The EPR signal from the ground state of V^- is quenched on illumination, and recovers on removal of the light. We define τ_q as the time constant for the decay of the EPR signal on light and τ_r as the time constant for the recovery when the light is switched off. Figure 9 shows that when the light is switched off the recovery (from its quenched level) of the V^- ground state EPR signal is much slower than decay of the EPR signal from the new center ($\tau_r \gg \tau_d$). Fitting the

TABLE II. The effect of light of a given excitation energy on the intensity of the EPR signal from V^- center. The sample was left in the dark at room temperature for several hours, and then illuminated in the sequence shown working down column 1. When illumination was applied or removed the signal came to equilibrium within 5 minutes and no further changes were observed.

| Excitation energy (eV) | Effect of light on V^- EPR signal | |
|---------------------------|--|-----------------------------------|
| | Temp = 298 K | Temp = 5 K |
| 2.85(5) | First Quenched (fast) then Enhanced (slow) (Light off no change) | Quenched (Light off no change) |
| 3.1(1) | Quenched (Light off small increase) | Enhanced (Light off no change) |
| 3.4(1) | Quenched (Light off enhanced) | Quenched (Light off enhanced) |
| 3.1(1) | Enhanced (Light off no change) | Enhanced (Light off no change) |
| 2.85(5) | Quenched (fast) \Rightarrow Enhanced (slow) (Light off no change) | Quenched (Light off no change) |

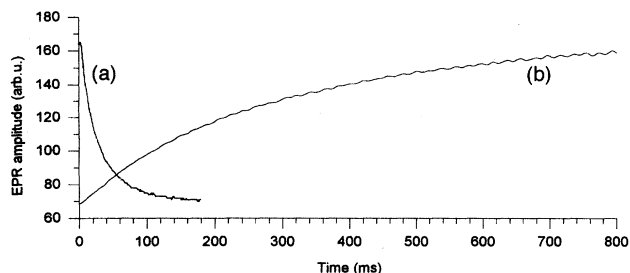


FIG. 9. Temporal dependence of V^- EPR signal on (a) illumination with full spectra of Hg lamp, or (b) subsequent removal of illumination. The Zeeman field is along [001] (set on lowest field nearest-neighbor ^{13}C hyperfine line), the microwave frequency is approximately 9.6 GHz, the incident microwave power is 0.3 mW, and the temperature approximately 5 K.

recovery to an increasing exponential function $(1 - \exp[-t/\tau_r])$ indicates that $\tau_r = 300(10)$ ms at 5.0 K. The quenching of the V^- EPR signal upon illumination is more rapid than the recovery. Fitting to a single exponential decay gives $\tau_q = 28(1)$ ms at 5.0 K, which is still slow compared with the changes in the EPR from the new center.

The decay of EPR signal from the single substitutional nitrogen center when the light is applied and the recovery when it is removed are slower than those of the V^- ground state EPR signal. Using the same notation as for V^- we find that upon illumination $\tau_q = 120(5)$ ms and removal of the light $\tau_r = 470(10)$ ms at 5.0 K.

E. ^{13}C ENDOR on the nearest neighbors and next nearest neighbors of the new center

ENDOR spectra were recorded from nearest-neighbor ^{13}C atoms of the new center while continuously illuminating with full spectra of Hg lamp at temperatures between 5.0 K and 100 K. The natural abundance of ^{13}C is only 1.11% and the ENDOR signal to noise was low. It was possible to make measurements on the large EPR transitions observed only when the Zeeman field is parallel to [100] or [111]. Accurate alignment of the sample was achieved using the EPR and ENDOR signals from the [N-C] 0 center. Figure 10 shows nearest-neighbor ^{13}C ENDOR transitions obtained, after signal averaging, while saturating the lowest field EPR transition labeled with an arrow in Fig. 3. The $S=2$ spin state is unambiguously identified by the appearance of pairs of lines centered approximately on A and $2A$ and separated by $2g_N\mu_N B$. A is the hyperfine splitting in a given orientation and $g_N = 1.404$ identifying the nucleus as ^{13}C . Simulations for other spin states are shown in Fig. 10. The hyperfine parameters determined by least squares fitting Eq. (1) to the ENDOR data, constraining the hyperfine interaction matrix to axially symmetry with the principal axis along [111], are given in Table I.

Figure 11 shows ^{13}C ENDOR from the next nearest neighbors while saturating the highest field EPR transition labeled with an arrow in Fig. 3. Again $S=2$ and $g_N = 1.404$ are confirmed by the pattern of lines. The ^{13}C ENDOR line shape for the next nearest neighbors reproduces the EPR line shape and is different from that obtained with the nearest

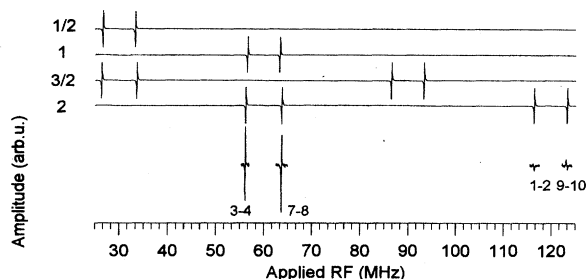


FIG. 10. Nearest-neighbor ^{13}C ENDOR from the 5A_2 excited state of V^0 . Zeeman field oriented along [001] (set on lowest field hyperfine line marked with an arrow in Fig. 4), microwave frequency 9.6 GHz, incident microwave power is 0.3 mW, rf power 50 W, temperature 5 K, and the sample illuminated with full spectrum of Hg lamp. Upper traces are simulations for different spin states, using parameters from Table I.

neighbors, which suggests that the ENDOR mechanism is different. The extra lines in Fig. 11 possibly originate from a more distant carbon neighbor, or even from a different center. It is clear from Fig. 3 that there are other EPR lines around $g=2.0033$ which are probably due to more distant ^{13}C neighbors.

We have assumed that the ^{13}C hyperfine interaction of the next nearest neighbors is axially symmetric with the principal axis along a [111] direction, because if the symmetry were lowered to σ_h (like that determined for the next nearest neighbors of V^- at 4 K) all the ENDOR lines in Fig. 11, except the one close to the nuclear Zeeman frequency, would be split into doublets with a 2:1 intensity ratio. The fact that the ENDOR transitions in Fig. 11 are not split indicates that axial symmetry is a good assumption. ENDOR measurements with the Zeeman field along [100] and [111] directions were least squares fitted to Eq. (1), assuming a [111] axially symmetric interaction, to produce the parameters in Table I.

IV. DISCUSSION

A. The 5A_2 excited state of the neutral vacancy

The EPR and ENDOR measurements show that the new center has tetrahedral symmetry and effective spin $S=2$, as

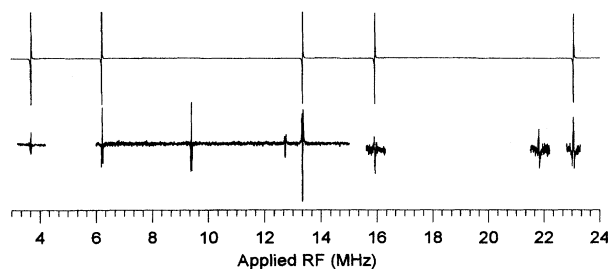


FIG. 11. Next-nearest-neighbor ^{13}C ENDOR from the 5A_2 excited state of V^0 . Zeeman field oriented along [001] (set on the highest field EPR transition marked with an arrow in Fig. 4), microwave frequency 9.6 GHz, incident microwave power 0.3 mW, rf power 50 W, temperature 5 K, and the sample illuminated with full spectrum of Hg lamp. Upper trace is a simulation with $S=2$ using parameters from Table I.

well as identifying the ^{13}C hyperfine coupling matrices for the nearest and next nearest neighbors. The stability of this defect to high temperature annealing indicates that it is substitutional rather than interstitial. We have no evidence that an impurity atom is incorporated in this defect and its creation immediately after irradiation suggests that it is a primary damage product.

The experimental evidence indicates that this center is an excited state of the neutral vacancy, the only possible $S=2$ spin state is the 5A_2 state. No $S=2$ state is possible for the $2+$, $+$, $-$ and $2-$ charge states of the vacancy. This identification confirms the prediction made by Coulson and Kearsley¹¹ and several subsequent calculations that the 5A_2 state is a low lying state located in the band gap.

The creation of the 5A_2 state correlates with loss of V^- on illumination. Since the GR1 uv band overlaps with the ND1 band, it is possible that the 5A_2 state is created by internal excitation of the V^0 center. However, the 5A_2 state has not been observed in diamonds containing V^0 and no V^- and it is well known that ionization of V^- produces V^0 .^{8,15} We do not know whether or not the 5A_2 state of V^0 is created uniformly throughout the sample, though it is clear that the distribution of V^- is not isotropic. We will postulate that the 5A_2 state is created via ionization of V^- , and consider the properties of this excited state in the following sections.

B. Selective population of different spin states and the EPR line shape

The EPR line shape (Fig. 3) and the angular variation of the EPR intensity (Fig. 4) from the 5A_2 excited state are unusual. The EPR line shape observed in Fig. 3 arises from anisotropic population of the different M_S levels in combination with small shifts in the positions of transitions between different $M_S \leftrightarrow M_{S+1}$ levels caused by second order terms in the hyperfine interaction [Eq. (1)].

Anisotropic populations of different M_S levels have been reported in studies on excited state $S=1$ triplets. The effect is apparent when the $|+1\rangle \leftrightarrow |0\rangle$ transition appears in emission (absorption) while the $|0\rangle \leftrightarrow |-1\rangle$ transition is in absorption (emission).³³⁻³⁵ The results indicate selective population (depopulation) of the state labeled $M_S = 0$ over the $M_S = \pm 1$ states. This phenomenon has been interpreted in terms of selective intersystem crossing from an excited singlet state (populated by an electric dipole transition) to specific M_S Zeeman sublevels of the triplet. The selective intersystem crossing originates from anisotropic spin-orbit coupling which arises from the preferential quenching the orbital angular momentum perpendicular to the crystal field axis.^{33,34} Watkins³⁴ pointed out that if the triplet were generated by capture of an electron or hole from the conduction or valence bands, rather than a localized excitation, then uniform population (ignoring the Boltzmann factor) of the triplet states would be expected. However, selective transitions out of the excited state triplet to a lower lying singlet state (originating via anisotropic spin-orbit coupling as discussed above) could generate a population inversion in the excited state.

It should be remembered that in order to see the EPR transitions in emission and enhanced absorption, it is neces-

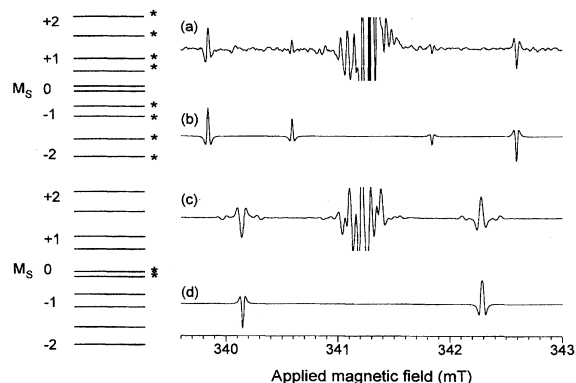


FIG. 12. Figures (a) and (c) are experimental EPR spectra from the 5A_2 state of the V^0 taken at 5 K with Zeeman field oriented along a $[110]$ and $[001]$ crystallographic axis, respectively. The microwave frequency was approximately 9.6 GHz and the sample was illuminated by the full spectrum from Hg lamp. Figures (b) and (d) are simulations of EPR lines in (a) and (c), respectively, arising from the hyperfine coupling to a single nearest-neighbor ^{13}C atom. For the simulations in (b) and (d) only the levels marked with a star in the adjacent schematic energy level diagram were assumed to be populated. See the text for further details.

sary that the spin-lattice relaxation time be similar to or longer than the triplet lifetime itself. The system studied here is different to the previously reported examples because we have a pentuplet ($S=2$) excited state rather than a triplet, and the symmetry is tetrahedral rather than axial. The structure of the spin-orbit coupling operator lets us predict the symmetry of the orbital states mixed by the orbital part of the perturbation. The orbital angular momentum operators transform as rotations, so for T_d symmetry they transform as the irreducible representation T_1 . Using the direct product rule we see that an A_2 state could contain an admixture of T_2 , but no other state to first order. Considering the spin part as well indicates that the only state mixed into the 5A_2 by spin-orbit coupling is 3T_2 .

We have not seen EPR from the 3T_2 state, possibly because its lifetime is too short. It is not yet clear how the 5A_2 state is created, or whether the anisotropic population is generated by selective transitions into or out of this state (or even in a preceding singlet-triplet transition). However, selective level population does explain the observed spectra. In Fig. 12 we have simulated the EPR spectra for the 5A_2 state of V^0 with a single ^{13}C nearest neighbor when the applied Zeeman field is parallel to the $[001]$ and $[110]$ crystallographic axes ($B\parallel[001]$ and $B\parallel[110]$) by making the following assumptions: (a) the levels marked with a star in Fig. 12 are equally populated, the others empty; (b) the EPR transition intensities are proportional to the transition probability and the population difference between levels; and (c) the line shape is Lorentzian (pseudomodulation³⁶ has been used to simulate the operation of the spectrometer). The agreement between the simulation and experiment is encouraging. The asymmetry between high and low field lines in the simulation with $B\parallel[110]$ is produced by the inclusion of the term in Eq. (2) ($a = 1$ MHz) in Eq. (1). This term produces shifts in the positions of the transitions that are less than those due to

the second order hyperfine terms but sufficient to modify the line intensities. This asymmetry is evident in the experimental data (Fig. 4) and supports the inclusion of the higher order term Eq. (2).

The line shape of the EPR transitions from the next-nearest-neighbor ${}^{13}\text{C}$ atoms (Fig. 5) arise in the same way as for the transitions from the nearest-neighbor ${}^{13}\text{C}$ atoms. However, the line at $g=2.0033(1)$ from excited state vacancies with no resolved hyperfine coupling does not behave in quite the same way. When the magnetic field is rotated in a $\{110\}$ plane the EPR lines are strongest with $\mathbf{B} \parallel [001]$ and decrease in intensity as the field is rotated away from this direction, disappearing when $\theta \approx 30^\circ$ because the different M_S states become equally populated. The relative positions of hyperfine lines from different sublevels is determined by the second order hyperfine terms, and the order of the transitions does not change as the magnetic field is rotated in the $\{110\}$ plane. However, on rotating beyond 30° from $[001]$ the population differences between the different M_S states change sign such that the hyperfine lines previously in absorption change to emission and *vice versa*. Thus at $\theta \approx 30^\circ$ the hyperfine lines in Fig. 4 change phase.

For the line at $g=2.0033(1)$ there is no hyperfine splitting and so we may expect the transitions in absorption and emission to superimpose and cancel, giving zero intensity in all orientations. We see a resonance because Eq. (2) splits the transitions from different M_S sublevels. This interaction vanishes at $\theta \approx 30^\circ$ and thus the transition goes to zero because of exact superposition of lines in emission and absorption. For $\theta > 30^\circ$ Eq. (2) changes sign and the relative positions of the transitions change: at the same time they switch from emission (absorption) to absorption (emission). Therefore the $g=2.0033(1)$ transition does not change phase as the field is rotated through 30° , it simply goes through a minimum in intensity. The differences in M_S populations appear to follow the term of fourth degree in the electrostatic potential. This term changes sign at $\theta \approx 30^\circ$, it is maximum along $[001]$ and is $-2/3$ ($-1/4$) times as large along $[111]$ ($[110]$). The intensities of the EPR transitions remain constant when the magnetic field is rotated in a $\{111\}$ plane; in this plane the potential [Eq. (2)] is constant.

C. The electronic g shift

Taken in isolation one would expect the angular momentum of the 5A_2 state to arise solely from the spin angular momentum. The g matrix would be isotropic and $g = g_e = 2.00232$. The measured deviation, $\Delta g = 0.0010(1)$, arises from a contribution of orbital angular momentum from other excited states. As discussed above the spin-orbit coupling operator mixes only the 3T_2 state into the 5A_2 state. Similarly the 4A_2 ground state of the V^- contains an admixture of 2T_2 . The g shift of the 4A_2 state is small, $\Delta g = 0.0004(1)$, because the spin-orbit coupling is weak and the separation of the 4A_2 and 2T_2 states large. A separation of 2 eV is estimated from the calculation of Lowther.³⁷ By analogy with Lowther's calculation we estimate from the measured g shift for the 5A_2 state that the 5A_2 and 3T_2 states are separated by about 1 eV.

D. The unpaired electron wave function

Following the usual linear combination of atomic orbitals procedure the unpaired electron wave function can in general be written as

$$\Phi = \sum_i \eta_i (\alpha_i \phi_{2s} + \beta_i \phi_{2p}), \quad (3)$$

where the summation is over the carbon atoms on which the unpaired electron is localized and ϕ_{2s} and ϕ_{2p} are the $2s$ and $2p$ atomic orbitals, respectively. The parameters α_i , β_i , η_i , taken to be real, are deduced in the usual way from the hyperfine parameters and the atomic parameters tabulated by Morton and Preston.³⁸ The hybridization ratio is $\lambda_i = \beta_i / \alpha_i$.

The simple one electron approach indicates that for the 5A_2 excited state of V^0 , and the 4A_2 ground state of V^- , 75% and 84%, respectively, of the unpaired electron spin density is located in the dangling orbitals of the four nearest neighbors. For both centers the magnitude of the anisotropic part of the hyperfine coupling with next-nearest-neighbor ${}^{13}\text{C}$ atoms is consistent with predominately dipolar coupling between the nucleus and the unpaired electron density in the dangling orbitals of the nearest neighbors.

Following a simple method for estimating displacements of atoms from the hybridization ratio,³⁹ we estimate that the nearest neighbors relax away from the vacancy by about 0.15 Å in the 4A_2 state of V^- and about 0.23 Å in the 5A_2 state of V^0 . The hyperfine parameters of the next nearest neighbors suggest that there is little distortion as well as very little localization of the unpaired electron density this far away from the vacancy.

E. Temperature dependence of V^0 excited state EPR

The EPR signal strength from 5A_2 state exhibits a marked temperature dependence first increasing as the temperature is reduced to about 100 K and then remaining constant down to 4 K. This is not a Curie Law dependence, neither is it that of a thermally excited state. If the M_S level populations are determined by spin-orbit coupling induced intersystem crossing then we would expect the relative populations, and hence EPR intensities, to be approximately temperature independent. However, we know that the EPR signal shape is produced by the addition of closely spaced lines in emission and absorption, which suggests that the signal strength would depend markedly on the EPR linewidth. We know that at helium temperatures the lifetime (τ_d) and spin-lattice relaxation time (T_1) are both long (T_1 must be greater than τ_d in order to see lines in emission). Therefore it is not possible for T_1 to determine the linewidth; but *lifetime* broadening is possible.

We simulated the EPR signal arising from nearest-neighbor ${}^{13}\text{C}$ hyperfine coupling ($\mathbf{B} \parallel [001]$) as a function of linewidth and obtained a relation between the half-width at half-height (of the components) and the peak-to-peak line height. After estimating a residual low temperature linewidth by simulating the EPR spectra, the linewidth of the component lines was calculated as a function of temperature. In Fig. 7(b) we plot the component linewidth against reciprocal temperature. At high temperatures an exponential behavior is

observed which can be modeled by an Arrhenius-type expression with an activation energy of about 40(5) meV. It is possible that as the temperature is increased thermal excitation from the 5A_2 state to a higher short lived state occurs. If this explanation is correct then the 5A_2 state is placed close to another midgap state with a short lifetime, perhaps 1T_2 . Without more information further speculation is unwarranted.

F. Lifetime and excitation energy dependence of the 5A_2 excited state EPR

The time taken for the 5A_2 EPR signal to decay on removal of uv light and the time for the signal to grow to its equilibrium value on application of uv light were shown to be equal at 5 K. The characteristic lifetime decreased with increasing microwave power and at vanishing low microwave power was about 9 ms. A long radiative lifetime is expected because optical transitions to lower lying states are spin forbidden and only gain intensity via spin-orbit coupling mixing states. Preliminary measurements indicate that the lifetime is temperature independent up to at least 80 K.

The maximum reduction in the concentration of V^- we have achieved by illumination with uv light is about 85–90 %. The creation of V^0 centers in excited states other than 5A_2 (which decay rapidly to the ground state avoiding the 5A_2 state) by V^- losing a t_2 electron is probably more likely than V^- losing an a_1 electron to create V^0 in the 5A_2 state. We have not been able to determine what fraction of V^- centers are ionized directly to the 5A_2 state. The fact that $\tau_d\{V^-\}$ is very much shorter than $\tau_g\{V^-\}$ is not surprising. Without illumination an equilibrium number of V^- and V^0 centers is eventually reached which depends on the number of electron donors and traps in the sample. On illumination with uv light V^- centers are ionized, and some of the electrons released may immediately recombine with V^0 centers, or be caught by other traps. The number of V^- centers does not fall as quickly as one might expect because new V^- centers can be created in this process. Eventually a new dynamic equilibrium is reached with fewer V^- centers, more V^0 centers, and traps which have captured an electron. When the light is switched off the electrons tunnel or hop back to V^0 centers from the electron traps and the original equilibrium number of V^0 and V^- centers is restored. The recovery in $[V^-]$ is much slower than the original decay because we are now dependent only on the lifetime of the traps and do not have the $V_1^- + V_2^0 + h\nu \Rightarrow V_1^0 + V_2^-$ processes contributing.

The single substitutional nitrogen center $[N-C]^0$ shows a similar behavior to the V^- center on illumination. The maximum reduction in $[N-C]^0$ we achieved was about 80% and the decay/recovery times were longer than those for V^- . The $[N-C]^0$ center is known to be an electron donor converting V^0 to V^- . We presume that on illumination with uv light $[N-C]^0$ can be ionized to $[N-C]^+$ with the extra electron being taken up by a trap. This trap is not a V^0 center because the number of V^- centers does not increase. The decay and recovery in the number of V^- and $[N-C]^0$ centers both fit to single exponential functions which is markedly different to the results on the $[N-N]^+$ center where the EPR signal decayed linearly with the logarithm of time on removal of the excitation.³⁹ This suggested that there was a wide distribu-

tion of lifetimes of the $[N-N]^+$ centers, presumably resulting from a large variation in the separation between the $[N-N]^+$ center and its electron donor and or trap. Further investigations of the decay and recovery times of the V^- and $[N-C]^0$ centers are planned.

Approximately the same number of ${}^5A_2 V^0$ centers are created with 3.1(1) and 3.4(1) eV light, whereas more V^- centers are quenched with the higher energy light. Not all V^- centers are converted to the 5A_2 state of V^0 . The effect of light of different energies depends on the state of preparation of the diamond. When light of a given energy illuminates the sample the V^- concentration is altered to an equilibrium level appropriate to the illumination; it may be quenched or enhanced to attain this concentration. The effect of 2.85 eV light is temperature dependent (Table II) and we note that this energy is well below the zero-phonon line of the V^- absorption.

We have a complicated system where electrons are transferred between different centers. Given our lack of knowledge of the traps and donors in the sample, the fact that the concentration of V^- is only a small fraction of the total defect concentration and the inhomogeneity in the sample, we have not attempted to investigate the processes in detail. The creation of the 5A_2 state by illumination with uv light is unusual. In most diamonds containing V^- and V^0 this excited state is not observed. The lifetime of the 5A_2 state may be related to the defect and impurity concentration in the diamond. Further study is required to investigate why this center is observed only in certain diamonds.

V. CONCLUSIONS

We have demonstrated that the new center observed on illumination with uv light is the 5A_2 state of the neutral vacancy. The unpaired electron population is predominantly located in the carbon dangling orbitals. The EPR line shape is produced by a combination of small shifts in the positions of transitions between different M_S states and the anisotropic population of the different states. The electronic g shift is satisfactorily explained by spin-orbit coupling mixing the 3T_2 state into 5A_2 . We estimate that the separation of the two levels is about 1 eV. Lifetime broadening of the EPR linewidth can be satisfactorily modeled with an Arrhenius-type expression with an activation energy of 40(5) meV. It appears that the 5A_2 state of the neutral vacancy is midgap, the reasons for its creation in the diamond studied here are not understood. Further work on the lifetime and creation of this center are required.

ACKNOWLEDGMENTS

O.D.T. thanks De Beers Industrial Diamond Division for support. We thank Dr. R. J. Caveney and his associates at De Beers Industrial Diamond Division for the provision of samples. We acknowledge the help of Dr. C. M. Welbourn and his colleagues at the Diamond Trading Company, Research Laboratory, Maidenhead, with sample preparation. We thank Professor J. A. Weil for the simulation and fitting software EPR.FOR, EPSRC (Grant No. GR/H33053) and the Department of Physics, Oxford, for financial support.

- *Author to whom correspondence should be addressed.
- ¹*Properties and Growth of Diamond*, edited by G. Davies (INSPEC: Institute of Electrical Engineers, London, 1994).
 - ²J. H. N. Loubser and J. Wyk, *Diamond Res.* **11**, 11 (1977).
 - ³X.-Fe. He, N. B. Manson, and P. T. Fisk, *Phys. Rev. B* **47**, 8809 (1993).
 - ⁴J. Isoya *et al.*, *Phys. Rev. B* **45**, 1436 (1992).
 - ⁵C. D. Clark, R. Ditchburn, and H. B. Dyer, *Proc. R. Soc. London Ser. A* **234**, 363 (1956).
 - ⁶C. D. Clark and J. Walker, *Proc. R. Soc. London Ser. A* **241**, 433 (1973).
 - ⁷G. Davies, *J. Phys. C* **7**, 3797 (1974).
 - ⁸G. Davies, *Chem. Phys. Carbon* **13**, 1 (1977).
 - ⁹G. Davies, in *Properties and Growth of Diamond*, edited by G. Davies (INSPEC: Institute of Electrical Engineers, London, 1994), Chap. 5.3.
 - ¹⁰J. E. Lowther, *Phys. Rev. B* **48**, 11 592 (1993).
 - ¹¹C. A. Coulson and M. J. Kearsley, *Proc. R. Soc. London Ser. A* **241**, 433 (1957).
 - ¹²A. Mainwood, J. Lowther, and J. van Wyk, *J. Phys. Condens. Matter* **5**, 7929 (1993).
 - ¹³G. Davies *et al.*, *Phys. Rev. B* **46**, 13 157 (1992).
 - ¹⁴G. Davies, *J. Phys. C* **3**, 3474 (1970).
 - ¹⁵H. B. Dyer and L. du Preez, *J. Chem. Phys.* **42**, 1898 (1990).
 - ¹⁶G. D. Watkins, *J. Phys. Soc. Jpn.* **18**, Suppl. II, 22 (1963).
 - ¹⁷G. D. Watkins, in *Radiation Damage in Semiconductors*, edited by P. Baruch (Dunod, Paris, 1965), p. 97.
 - ¹⁸G. D. Watkins, in *Radiation Damage and Defects in Semiconductors*, edited by J. E. Whitehouse (Institute of Physics, London, 1973), p. 228.
 - ¹⁹M. Sprenger, S. H. Muller, E. G. Sieverts, and C. A. J. Ammerlaan, *Phys. Rev. B* **35**, 1566 (1987).
 - ²⁰G. Davies, *Rep. Prog. Phys.* **44**, 787 (1981).
 - ²¹G. D. Watkins, *Defects in Semiconductors* (Institute of Physics, London, 1972), p. 228.
 - ²²G. D. Watkins, in *Lattice Defects in Semiconductors*, edited by F. A. Huntley (Institute of Physics, London, 1975), p. 1.
 - ²³K. L. Brower, *Phys. Rev. B* **1**, 1908 (1970).
 - ²⁴G. D. Watkins and J. R. Troxell, *Phys. Rev. Lett.* **44**, 593 (1980).
 - ²⁵G. D. Watkins, A. P. Charterjee, and R. D. Harris, in *Defects and Radiation Effects in Semiconductors 1980*, edited by R. Hashiguchi (Institute of Physics, London, 1981), p. 199.
 - ²⁶J. L. Newton, A. P. C. R. D. Harris, and G. D. Watkins, *Physica B* **116**, 219 (1983).
 - ²⁷J. A. van Wyk and G. S. Woods, *J. Phys. Condens. Matter* **7**, 5901 (1995).
 - ²⁸G. S. Woods, G. C. Purser, A. S. Mtimkulu, and A. T. Collins, *J. Phys. Chem. Solids* **51**, 1191 (1990).
 - ²⁹G. Davies, A. T. Collins, and P. Spear, *Solid State Commun.* **49**, 433 (1984).
 - ³⁰G. Davies and M. F. Hamer, *Proc. R. Soc. London Ser. A* **348**, 285 (1976).
 - ³¹W. V. Smith, P. P. Sorokin, I. L. Gelles, and G. J. Lasher, *Phys. Rev.* **115**, 1546 (1959).
 - ³²EPR.FOR (version 5.13); D. G. McGavin, M. J. Mombourquette, and J. A. Weil. Inquiries should be made to Professor J. A. Weil, Department of Chemistry, University of Saskatchewan, Saskatoon, SK, S7N 0W, Canada. Electronic address: WEIL@SASK.USASK.CA
 - ³³D. H. Tanimoto, W. M. Ziniker, and J. O. Kemp, *Phys. Rev. Lett.* **14**, 645 (1965).
 - ³⁴G. D. Watkins, *Phys. Rev.* **155**, 802 (1967).
 - ³⁵K. L. Brower, *Phys. Rev. B* **4**, 1968 (1971).
 - ³⁶J. Hyde, M. Pasenkiewicz-Gierula, A. Jesmanowicz, and W. Antholine, *Appl. Magn. Reson.* **1**, 483 (1990).
 - ³⁷J. E. Lowther and J. A. van Wyk, *Phys. Rev. B* **49**, 11 010 (1994).
 - ³⁸J. Morton and K. Preston, *J. Magn. Reson.* **30**, 577 (1978).
 - ³⁹O. D. Tucker, M. E. Newton, and J. M. Baker, *Phys. Rev. B* **49**, 15 586 (1994).